Programming the mechanics of cohesive fiber networks by compression†

Bart E. Vos,[a] Luka C. Liebrand,[b,‡] Mahsa Vahabi,[b] Andreas Biebricher,[b] Gijs J. L. Wuite,[b] Erwin J. G. Peterman,[b] Nicholas A. Kurniawan,[c] Fred C. MacKintosh,*[b,d,e] and Gijsje H. Koenderink*[a]

Fibrous networks are ideal functional materials since they provide mechanical rigidity at low weight. Here, we demonstrate that fibrous networks of the blood clotting protein fibrin undergo a strong and irreversible increase in their mechanical rigidity in response to uniaxial compression. This rigidification can be precisely controlled by the level of applied compressive strain, providing a means to program the network rigidity without having to change its composition. To identify the underlying mechanism we measure single fiber-fiber interactions using optical tweezers. We further develop a minimal computational model of cohesive fiber networks that shows that stiffening arises due to the formation of new bonds in the compressed state, which develop tensile stress when the network is re-expanded. The model predicts that the network stiffness after a compression cycle obeys a power-law dependence on tensile stress, which we confirm experimentally. This finding provides new insights into how biological tissues can adapt themselves independently of any cellular processes, offering new perspectives to inspire the design of reprogrammable materials.

1 Introduction

Fibrous materials are ubiquitous in biology, forming the structural framework of cells and connective tissues[1]. Similar design principles are also harnessed in many man-made materials ranging from paper and textiles to light-weight composites[2]. Fibrous networks are superior functional materials, since stiff polymers and rigid fibers can form space-filling elastic networks at exceedingly low volume fractions of less than 1%, and at low connectivities where only 3 to 4 fiber segments meet at each node. This connectivity is below the Maxwell isostatic threshold for simple spring networks, which requires a connectivity of at least 6 for a mechanically stable network[3]. Fibrous materials can beat this threshold, due to the stabilizing effects of stress and the large bending resistance of fibers[4–7]. Moreover, the stiffness of fibrous networks is sensitive to the density of cross-linkers between fibers[8]. Such networks also reversibly stiffen under shear or tensile deformation, a phenomenon that has been explained by network models consisting of either semiflexible or elastic fibers[5,6,9]. These properties in principle allow one to adjust the stiffness of fibrous networks to specific functional requirements. However, they offer only limited options for *in situ* adjustment since changing crosslink density requires making a new system for each application, while strain-stiffening is only operative as long as a mechanical strain is applied.

Nature has found intriguing ways to adapt the mechanical performance of fibrous networks in tissues in a more dynamic fashion to diverse and time-varying mechanical loading conditions. Tissues are able to actively reinforce their structure along the principal load direction. The mechanisms of mechanical reinforcement are generally thought to originate from cellular activity, involving strain-dependent fiber degradation and synthesis[10,11]. However, recent studies suggest that biopolymer networks are inherently adaptive themselves, since they are held together by weak transient bonds[12,13]. Cyclic shear loading has been shown to cause reinforcement for a number of biopolymer systems[14–17], al-

[a] *Biological Soft Matter group, AMOLF, 1098XG Amsterdam, The Netherlands; E-mail: g.koenderink@amolf.nl*

[b] *Department of Physics and Astronomy, Vrije Universiteit, 1081HV Amsterdam, The Netherlands.*

[c] *Department of Biomedical Engineering & Institute for Complex Molecular Systems, Eindhoven University of Technology, 5612AZ Eindhoven, The Netherlands*

[d] *Departments of Chemical & Biomolecular Engineering, Chemistry, and Physics & Astronomy, Rice University, Houston, TX 77005, USA; E-mail: fcmack@rice.edu*

[e] *Center for Theoretical Biological Physics, Rice University, Houston, TX 77030, USA*

† Electronic Supplementary Information (ESI) available: Estimation of fiber-fiber interaction strength by αC-regions; Movie 1: Direct measurement of the interaction between two individual fibrin fibers by optical tweezers; Movie 2: Two junctions merging in our computational model of cohesive fibrous networks; Supporting figures: Normal force relaxation, FXIII-inhibition, Confocal rheology, Simulation data. See DOI: 10.1039/b000000x/

‡ Present address: Department of Psychiatry, Academic Medical Center, University of Amsterdam, The Netherlands

though softening can occur as well[18,19]. The physical principles responsible for these varied inelastic responses are still not fully understood, although possible mechanisms include bond breaking and reformation between fibers[13,19,20] and within fibers[18].

To test the influence of cyclic loading on the inelastic behavior of fibrous networks, we choose fibrin as a model biopolymer (Fig. 1c) whose elastic properties have already been extensively studied in the context of blood clotting[21]. We show that fibrin networks undergo strong and irreversible stiffening when subject to axial compression. We apply a compressive strain, since this mode of deformation is most adept for strain-induced programming due to the volume-reducing nature of the deformation[22,23]. This is in contrast with most studies on intra- and extracellular matrices, which focused on shear deformation. However, *in vivo* all modes of deformation occur (compression, extension and shear).

By directly measuring the interactions between individual fibrin fibers using optical tweezers, we identify new bond formation as a possible origin for this stiffening. We develop a minimal computational model of cohesive fiber networks to show that bond remodeling can indeed explain reinforcement of fibrin networks under compression. Moreover, this model reveals that the strong degree of stiffening we observe can arise from a surprisingly small fractional increase in network bonds, due to the pre-stressed nature of new bonds formed under compressive loading. Our model predicts a power-law dependence of the stiffening on the resulting contractile prestress, which we confirm experimentally. The generality of the stiffening of cohesive fiber networks, together with its predictable and reproducible dependence on compression, can be used as a basis for *in situ* programming the mechanics of fibrous materials by purely mechanical means.

2 Materials and Methods

2.1 Fibrin network rheology

We purchased chemicals from Sigma Aldrich (Zwijndrecht, Netherlands), human plasma fibrinogen and α-thrombin from Enzyme Research Laboratories (Swansea, United Kingdom), and fibrinogen labeled with the fluorophore Alexa488 from Life Technologies (Eugene, OR, USA). Rheological experiments were performed using an Anton-Paar rheometer (Physica MCR501, Graz, Austria) equipped with a 40 mm stainless steel parallel plate geometry to allow variation of the gap size. Samples were prepared by diluting fibrinogen stock solution (dialysed against a 150mM NaCl, 20mM HEPES, pH 7.4 buffer) to 2 mg/ml in an assembly buffer to obtain final concentrations of 150mM NaCl, 20mM HEPES and 5mM $CaCl_2$ at a pH of 7.4. Polymerization was initiated by addition of 0.5 U/ml thrombin. Directly after mixing, we transferred the solution to the bottom plate of the rheometer and lowered the top plate to reach a gap size of 1.0 mm. During polymerization, the temperature was kept constant at 22°C, and solvent evaporation was prevented by adding a layer of mineral oil (M3516, Sigma Aldrich) on the liquid-air interface. We checked that the oil layer did not influence the mechanical behavior of the networks.

During polymerization, we continuously measured the shear modulus, to verify that there was no evaporation or other disturbances of the sample. To this end, we applied a small oscillatory shear strain with an amplitude of 0.5% and a frequency of 0.5 Hz, and measured the shear stress response. Polymerization was complete after 10 hours as indicated by a time-independent shear modulus. Compression was achieved by lowering the top plate at a slow rate of 1 μm/s in steps of 100 μm, corresponding to strain steps of 10%. In between each compression step, we held the gap fixed for 125 s to allow the normal force to equilibrate. Figure 1 in the Supplementary Information†shows a typical example of the relaxation of the normal force during and after compression, which we associate with poroelastic behavior. The time scale of the relaxation process is quite fast, on the order of 13 s,[24] reflecting the large (micron-scale) mesh size of the fibrin networks. We then measured the shear modulus of the equilibrated network by applying a small oscillatory shear strain (amplitude $\gamma = 0.5\%$ and oscillation frequency $\nu = 0.5$ Hz). Stepwise compression was continued until the thickness of the gel was reduced to 0.2 mm, corresponding to 20% of the original height and an axial strain of 80%. After compression, the gap was increased back to 1 mm (corresponding to an axial strain of zero) in a similar stepwise manner, and again allowing enough time for buffer to re-enter the network. We observed a residual tensile normal force (see Fig.1d), indicative of good adherence of the network to the rheometer plates and in line with earlier reports where high (shear) stresses were applied without requiring prior treatment of the rheometer surfaces (e.g.[25]). As a more rigorous test for strong enough plate adhesion, we also performed uniaxial extension tests in the rheometer. We found that the fibrin gels could be stretched by axial strains of at least 50%, corresponding to tensile stresses of at least 1.4 N, well above the stress levels (ca. 0.6 N) relevant throughout this work. We verified by UV-VIS absorption measurements of the expelled buffer solution that no protein was released from the networks during compression. In some experiments cross-linking by FXIII was inhibited by the addition of D004 (Zedira, Darmstadt, Germany) to the fibrinogen solution in a 30 to 1 molar ratio prior to the addition of thrombin[26]. For the rheology experiments, data points show the average of three measurements with error bars representing the standard deviation.

2.2 Optical tweezers

Optical tweezers experiments were performed using a custom-built four-trap optical tweezers system, combined with fluorescence microscopy. The sample chamber was a microfluidic flow cell with three inlets. Laminar flow conditions ensured that no mixing of the channels occurred. The first inlet contained 4.5 μm diameter spherical polystyrene beads (Spherotech, Lake Forest, IL, USA), which were trapped by a 20 W infrared ($\lambda = 1064$ nm) laser. The second inlet contained fibrin fibers, obtained by adding 0.5 U/ml thrombin to a 0.01 mg/ml fibrinogen solution where 10% of the monomers was labeled with Alexa-488. The third inlet contained just assembly buffer, which was supplemented in some experiments with the FXIII inhibitor D004. To test whether fibrin fibers are able to form bonds when brought in contact, we first trapped four beads in the bead channel, and next captured

two fibrin fibers in the fibrin channel by connecting them end-to-end to a bead pair, using the ability of fibrin to strongly adhere to polystyrene beads[27]. Finally, the two fibers were moved to the buffer channel using the beads as handles and one fiber was positioned underneath the other one by defocusing the trapping lasers and oriented in a crossed configuration. All beads were then brought back to the same focal plane in order to bring the fibers in contact. To test for fiber cohesion, we moved one of the bead pairs and performed time-lapse fluorescence imaging while concurrently measuring the force response on the other bead pair using a position-sensitive diode.

2.3 Confocal microscopy

Confocal microscopy was performed on a Nikon Eclipse Ti inverted microscope equipped with a 100x oil-immersion objective (NA = 1.40). Fibrinogen labeled with Alexa Fluor 488 (Life Technologies, Bleiswijk, The Netherlands) was mixed with unlabeled fibrinogen in a 1:19 molar ratio. Samples were prepared in glass chambers made of a microscope coverslip and slide with Parafilm spacers. Polymerization occurred at room temperature for at least 12 hours. Maximum intensity projections were made of a stack of confocal slices acquired over a depth of 10 μm.

Confocal microscopy in combination with compression was performed on a home-built setup, consisting of an Anton Paar rheometer head (DSR 301, Graz, Austria) placed on top of an inverted microscope equipped with a Yokogawa CSU-22 spinning disk confocal head, a Hamamatsu EM-CCD C9100 Digital Camera, and a 100x oil-immersion objective. The bottom plate consisted of a microscopy coverslip, while the top plate was a 20 mm stainless steel plate. The gap height was adjusted manually by moving the rheometer head up and down with a micrometer screw. The molar ratio of fluorescently labelled to unlabelled fibrinogen monomers was adjusted to 1:9, allowing shorter exposure times and reduced photobleaching.

2.4 Simulations

Disordered 2D lattices were generated by modifying triangular lattices with a lattice spacing of l_0 such that at each lattice vertex, one out of three passing filaments is randomly freed up[28]. This phantomization procedure sets the average connectivity (local coordination number) of the network to $z = 4$. We further diluted the network by random removal of fiber segments until the average connectivity, $\langle z \rangle$, reached a value between 3 and 4 that is typical of biopolymer networks. Biopolymer networks of fibrin, collagen and actin usually exhibit combinations of fiber branching ($z = 3$) and cross-linking ($z = 4$)[29]. This average connectivity is below the point of marginal stability for a network of Hookean springs with only stretching interactions. This isostatic connectivity is $2d_s$ where d_s is the dimensionality of the system[30]. Spring networks are floppy below this threshold, but they can be stabilised by introducing a bending rigidity or by applying an internal or external stress[4–6,31–34]. Here, we include bending interactions in the Hamiltonian of the system to account for the finite rigidity of fibrin fibers. Thus, the filaments in the network are described by the Hamiltonian

$$H = \sum_f \left[\int \frac{\kappa}{2} \left| \frac{d\hat{t}}{ds_f} \right|^2 ds_f + \int \frac{\mu}{2} \left(\frac{dl}{ds_f} \right)^2 ds_f \right] \qquad (1)$$

where the first term accounts for bending and the second term accounts for stretching. The summation is over all filaments in the system, $\hat{t}$ is the unit tangent along the filament and dl/ds_f is the longitudinal strain at point s_f along the fiber contour. Each fiber is assigned a bending rigidity κ and stretch modulus μ. Note that the simulations assume an athermal network, which is appropriate for rigid biopolymers such as collagen, fibrin, microtubules, and actin bundles. We set the dimensionless fiber rigidity, defined as $\tilde{\kappa} = \kappa/(\mu l_0^2)$ where l_0 is the lattice spacing, to 10^{-4}, a value that is appropriate for fibrin networks at the protein concentrations we are working at. The fiber rigidity is a dimensionless quantity that quantifies the relative importance of bend and stretch energy contributions and it is expected to vary approximately linearly with protein concentration assuming that the network architecture is invariant[5,6]. Simulation results shown in Fig. 3 have a capture radius of $d = 0.01 l_0$; simulations results shown in the Supplementary Information†have a capture radius of $d = 0.001 l_0$. The simulation results shown in Fig. 3 are an ensemble average of a total of ten different random networks.

3 Results

We polymerize fibrin networks between the plates of a shear rheometer and compress each network stepwise in increments of 10% axial strain, relative to the initial state. After each compression step, we return the sample to the initial (0% axial strain) state, for a complete compression cycle. We define the compressive strain by $\varepsilon = \frac{L_0 - L}{L_0}$, where L_0 is the initial sample height and L is the sample height under compression. Importantly, this definition of strain is not with respect to the relaxed state of the sample, which changes during a compression cycle. We perform each (de)compression step at a slow rate to allow for water efflux and influx (Fig. 1e). Furthermore, we allow the network to equilibrate for at least 125 seconds until the normal force exerted by the network on the rheometer top plate reaches a constant level (Fig. S1†). We probe the rigidity of the network at different levels of axial strain by measuring the shear modulus with a small amplitude oscillation. As we compress the network to increasing axial strains, the shear modulus progressively decreases (Fig. 1a, black). This softening response is consistent with previous studies of fibrin[22,23,35] and actin[36] and may indicate fiber buckling[35,37–39]. Even for pure spring networks, however, extension tends to stabilize networks while compression tends to destabilize networks[40,41]. At the highest maximum compressive strains that we apply (80%), there is a slight upturn of the modulus, possibly reflecting network densification[23,38,39].

When we decompress the network to its original height, we observe a strong increase in the shear modulus compared to the virgin state (Fig 1a), accompanied by an increased residual normal stress (Fig. 1d; the normal stress σ_n is the measured normal force F_n divided by the rheometer plate surface area). The increase is already more than twofold when the network has experienced a

compressive strain of 10% and rises to eightfold when the network has experienced a compressive strain of 80%. Importantly, the shear modulus reached after decompression is constant over time, so the compressive programming is irreversible.

To test whether the loading history affects the inelastic response, we also subjected networks to a single cycle of compression and decompression (Fig. 1a, red; Fig. 1e). The softening upon compression and stiffening upon decompression are nearly identical to the changes observed in the stepwise programming protocol, suggesting that only the maximum compressive strain that the sample has experienced is relevant, while the subsequent strain history plays no role. This conclusion is further supported by repeating cycles of compression to 80% strain and decompression to 0% strain, where we observe that the once-programmed network switches between the same high stiffness at 0% strain and low stiffness at 80% strain in subsequent cycles (Fig. 1b).

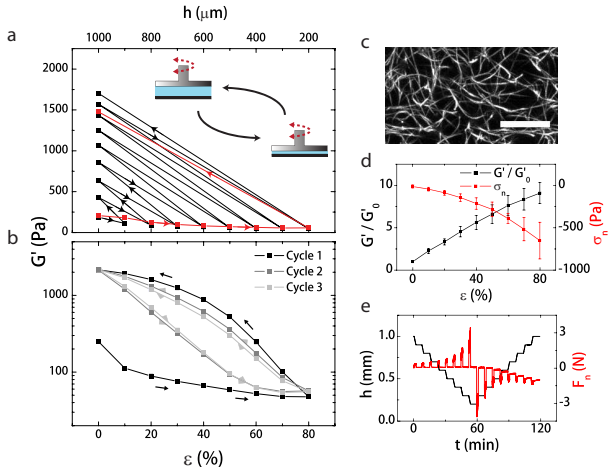

Fig. 1 a, Shear modulus G' of a fibrin network as a function of compressive strain ε and corresponding sample height h. The inset shows how the shear modulus is obtained by applying a small oscillatory shear strain while varying the axial strain. The black curve is obtained by cyclic loading-unloading in strain steps of 100 μm, while the **red** curve was obtained by directly compressing to $\varepsilon = 80\%$. **b**, Repeated compression to 80% strain and decompression, showing the first (black), second (grey) and third (light grey) cycle. **c**, Maximum intensity projection of a stack of confocal images of a fibrin network, acquired over a depth of 10 μm; scale bar, 10 μm. **d**, Normalized network stiffening G'/G'_0 and residual normal stress σ_n as a function of the maximum compressive strain ε that the network has experienced. **e**, Gap size h and normal force F as a function of time t during a single compression-decompression cycle. Arrows indicate the sequence of the compression-decompression steps. Error bars represent standard deviations.

The strong irreversible stiffening of the fibrin networks upon axial compression suggests that the structure of the network is being remodeled. A plausible hypothesis is that the fibers form additional bonds during compression, since compression increases the fiber density and thereby enhances the chance of fiber-fiber interactions. To test this hypothesis, we use a recently developed quadruple optical tweezers assay to directly probe the interaction between two individual fibrin fibers [13,42,43]. Using a microfluidic flow cell with separate inlets for a dilute suspension of 4.5 μm-sized polystyrene beads, a dilute solution of fluorescently labeled fibrin fibers, and assay buffer, we first capture four beads in the traps, then suspend a fibrin fiber between each bead pair, and move the two fibers into the buffer channel. We next bring the fibers in a crossed configuration by rotating one fiber (vertical in the fluorescence images in Fig. 2a), bringing it underneath the second, horizontally oriented fiber, and finally moving it upwards into contact with the horizontal fiber. To test whether the fibers spontaneously bond, we pull on the vertical fiber. As shown in Fig. 2a and the corresponding Supplementary Movie 1†, pulling on the vertical fiber causes displacement of the horizontal fiber. This observation provides clear evidence that the fibers spontaneously form bonds when brought in contact. To measure the bond strength, we monitor the force on the trapped beads. The red curve in Fig. 2a shows the force as a function of time on the beads connecting to the horizontal, stationary fiber, while the blue curve corresponds to the vertical fiber. Each time we pull on the vertical fiber, there is a corresponding force increase on the horizontal fiber until, at a force of 259 pN, the uppermost bead is pulled out of the trap. Indeed, we observe consistently (10 independent experiments) that the bead is pulled out of the trap while the connection between the fibers remains unbroken. As the trap strength is in the range of 300-400 pN, the tweezers measurements set a lower limit on the strength of the newly formed fiber-fiber junction of 343 ± 104 pN.

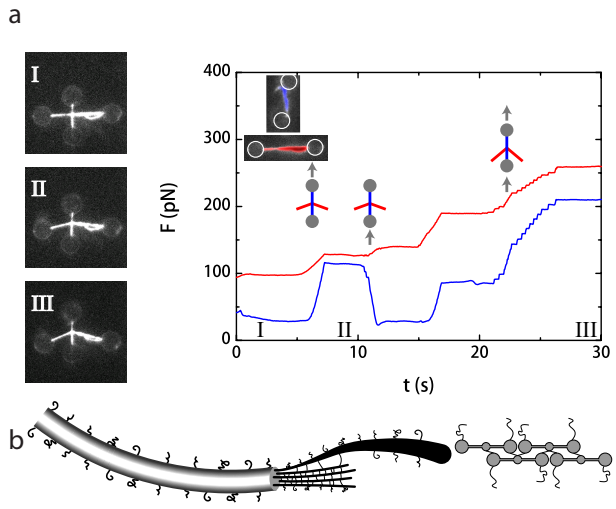

Fig. 2 a,Fluorescence microscopy images (left) and force F versus time t graph (right) for a typical optical tweezers experiment, using the same methodology as in [13], taken at time points indicated in the graph. Two fibers are crossed and brought into contact using four optically trapped beads as handles. After the vertically oriented fiber (blue) is brought in contact with the horizontally oriented fiber (red) (I), there is a force response on both fibers when the upper or lower bead of the vertical bead pair is moved. A movie showing the entire time-lapse sequence can be found in the Supplementary Information†. **b**, Schematic of the hierarchical organization of a fibrin fiber, with monomers (right) forming protofibrils (middle), and protofibrils forming bundles interconnected by the unstructured αC-regions (left).

What is the molecular mechanism of new bond formation? Fibrin fibers are thick bundles of around 65 double-stranded protofibrils held together by covalent and noncovalent interactions [13]. We polymerize fibrin in the presence of FXIII, a physi-

ologically important enzyme that stabilizes blood clots by generating covalent peptide bonds between fibrin monomers. A possible origin of the spontaneous fiber bonding could be the creation of new cross-links by fibrin-bound FXIII as the fibers are brought in contact. To test this idea, we repeated the fiber interaction measurements in the presence of the specific FXIII inhibitor D004[26]. We again observed strong fiber-fiber cohesion (Fig. S2†) and consistent with this, we find that inhibition of FXIII crosslinking activity does not change the extent of network stiffening after compressive loading (Fig. S3†). We conclude that FXIII induced cross-linking is not responsible for bond formation. Instead, we propose that bond formation is facilitated by noncovalent interactions, most likely mediated by the unstructured αC-regions, two long and flexible chains attached to the distal ends of each fibrin monomer[44]. Specific interactions between these chains mediate lateral association of protofibrils into fibers as well as interactions between fibrin fibers[45] (see schematic in Fig. 2b). We estimate that the total binding force between two interacting fibers mediated by adjacent αC-regions is approximately 760 pN, sufficient to account for the absence of junction rupture in the optical tweezers experiments, and the irreversibility of bond formation in the network-scale experiments (see the Supplementary Information†for the detailed calculation).

4 Simulations

These observations of new bond formation suggest a mechanism for fibrin network reinforcement by compressive loading. To address this, we develop a computational network model that allows for new bond formation under deformation†[28]. Fibrous networks are modeled as a 2D triangular disordered lattice with lattice spacing l_0 and dimensions of $50l_0 \times 50l_0$. We perform 2D simulations for computational efficiency, which is justified by recent studies showing that subisostatic fiber networks in 2D are surprisingly predictive of 3D behavior for the same connectivity z[5]. The average coordination number is adjusted to a physiologically relevant value of 3.4 to reflect the combination of branches and cross-links in networks such as fibrin. This is done by a combination of phantomization, a computational procedure to reduce the local connectivity of triangular networks from 6 to a maximum of 4, and dilution (for details, see the Supplementary Information†). Similar to the experiments, the lattices are compressed in steps of 1% from an initial axial strain of 0% to 50% and back to 0%. The fibers are modeled as elastic beams with a stretching modulus μ and bending modulus κ. We performed simulations for a fixed fiber rigidity, $\tilde{\kappa} = \kappa/\mu l_0^2 = 10^{-4}$, in the relevant range for fibrin networks. After each (de)compression step, we minimize the energy of the network and determine the normal and shear stresses from the variation of the energy with strain. Periodic, Lees-Edward boundary conditions are used to minimize boundary effects. To allow for network remodeling, we introduce a single midpoint between adjacent network nodes and allow two midpoints to merge into one node when applied deformations force them to approach one another to within a predetermined capture radius d, which we will refer to as the remodeling distance. In our simulations we choose $d = 0.01l_0$. Fig. 3a illustrates a merging event in half a unit cell of the lattice. The additional bond is added at the point indicated by the gray arrows. The bend and stretch moduli for the fiber segment shown by the thick vertical line both change by a factor of 2. The capture radius d does not really correspond to a new structural parameter but primarily controls the probability of bond formation. In developing the model, we confirmed this by varying independently d and a separate binding probability, with no significant differences between these two control parameters. In our simulations we choose $d = 0.01l_0$ to ensure sufficiently dilute new bond formation to be consistent with the degree of stiffening observed experimentally. Higher values of d increased the probability of new bond formation and were found to lead to higher levels of stiffening at lower levels of compression, although the results were otherwise qualitatively consistent with our experiments.

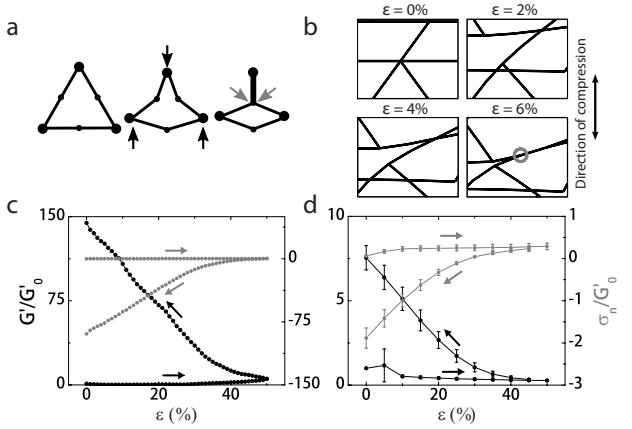

Fig. 3 a, Half a unit cell of our simulated fibrous lattice. Under compression (black arrows), two nodes within a remodeling distance $d = 0.01l_0$ merge (gray arrows). **b**, A small section of a simulated network during compression, shown up to the moment where the first merging event occurs (encircled in gray). A movie showing a complete compression sequence can be found in the Supplementary Information†. **c**, Shear modulus (black) and corresponding normal stress (gray) as a function of compressive strain for a simulated network ($\tilde{\kappa} = 10^{-4}$) and **d**, a fibrin network. Both axes are normalized by the initial shear modulus. Arrows indicate the sequence of the compression-decompression steps. Error bars represent standard deviations.

A typical remodeling event during the first steps of compression is highlighted in Fig. 3b, which shows a zoomed-in section of a simulated network. A non-trivial combination of bending and stretching of individual fibers brings two midpoints to within the remodeling distance, encircled in gray. Supplementary Movie 2†shows how the network as a whole responds to the applied compression. With increasing compressive strain, the simulations predict an initial softening, followed by stiffening when the axial strain reaches ca. 30% (Fig. 3c, black circles). Upon decompression to the initial network height, the simulations reveal a strong increase of the shear modulus by a factor 140, while the density of nodes has increased by only a factor 1.32, suggesting that high levels of stiffening are possible with only a modest increase in cross-linking. We find good qualitative agreement with experiment in the dependence of both the normal stress and shear modulus on compressive strain, as shown in Fig. 3d.

The extent of stiffening observed in simulations is sensitive to the remodeling distance d: for a ten-fold decrease in d ($d = 0.001 l_0$) the stiffening factor is ~10-fold, consistent with what we observe experimentally for fibrin networks. Importantly, this level of increase in stiffness is accompanied by only ~1.3% increase in cross-link density†. To verify this, we performed confocal imaging on a network (1) at rest, (2) under compression and (3) after decompression (see Supplementary Information†). We indeed observe no pronounced difference between the network structure before compression and after the compression/decompression cycle, confirming the model prediction that stiffening occurs with only a small increase in cross-linker density.

From the simulations, we obtain further insight into the mechanism of stiffening by considering the normal (axial) stress. New bond formation under compression is accompanied by a change in the relaxed state of the sample. After compression, the sample is returned to its initial height (Fig. 1a schematic). As this is done, we observe the development of tensile normal stress in the decompressed network (Fig. 3c, gray circles). Our experiments exhibit similar normal stress behavior, as shown in Fig. 3d. In our simulations, we can identify this tensile stress as arising from tensile forces in the decompressed network, resulting from the newly formed bonds. Thus, the residual axial stresses in the decompressed state are consistent with contractile forces acting on the initial network.

To test whether these contractile forces can account for network stiffening in our computational model, we plot in Fig. 4 the relative increase in shear modulus against the residual normal stress for networks exposed to different levels of axial strain (open symbols). Interestingly, we find not only a strong correlation between the normal stress and the increase in network stiffness, but this relationship is characterized by a sublinear or fractional power-law with exponent $\simeq 0.5$. Such a fractional power-law dependence is also observed in our experiments (filled symbols). Importantly, since both axes have been normalized by the initial linear shear modulus before compression, which can be independently determined in simulation as well as experiment, this provides a direct quantitative comparison between our experiments and our computational model: there are no adjustable parameters in this plot. While there is a small systematic difference between the simulations and experiments, both show a clear and consistent sublinear behavior with exponent $\simeq 0.5 - 0.6$.

The simulations demonstrate the role of the new bonds formed by compressive training is not simply to provide new network constraints. Rather, the new bonds cause stiffening because they provide contractile forces. It is well-known from previous theoretical work that fibrous networks are highly nonlinear in their elastic response,[1,2,46–48] so even dilute contractile force centers in the network can result in a significant change in the macroscopic network response. In prior work, this effect was demonstrated for the case of active contractile centers provided by molecular motors[28,32]. Here we show a new mechanism by which the same effect can occur in a purely passive system without motors. Network compression effectively creates contractile centers since new bonds that are formed in the strained state get extended when the network is decompressed. Specifically, it was recently predicted that randomly distributed contractile forces in subisostatic networks such as ours can result in a sublinear increase in G' with contractile stress[32]. While this work aimed to address stiffening by molecular motors, an increase in $G' \sim \sigma^y$ with contractile stress σ was found, with exponents y ranging from $0.6 - 0.8$ depending on network connectivity z. For $z \simeq 3.4$, comparable to what we expect for fibrin networks, $y \simeq 0.6$ was found, which is consistent with a fit to our experimental results in Fig. 4.

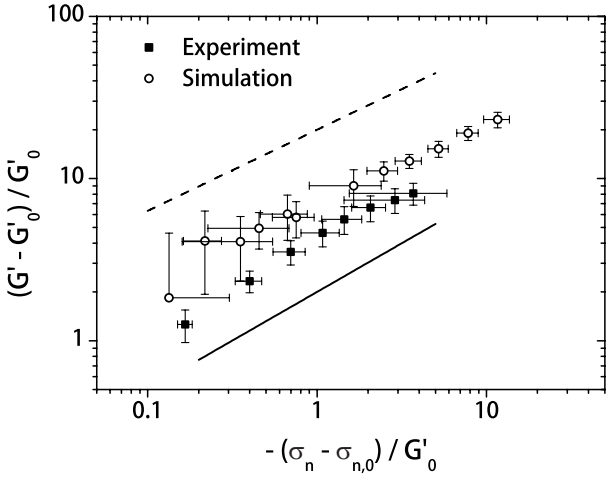

Fig. 4 Relative increase in the shear modulus with normal stress for a fibrin gel (black squares) and a simulated network with $\tilde{\kappa} = 10^{-4}$ (open circles) trained by compressing to different levels of axial strain. The initial network parameters (G'_0, $\sigma_{n,0}$) are subtracted, and the data are normalized by dividing by G'_0. We find power-law scaling with a slope between 0.6 (black line) and 0.5 (dashed line), only to guide the eye. Error bars represent standard deviations.

5 Conclusions

We find that networks of cohesive fibers stiffen under cyclic compressive loading and that this can be understood by the formation of new bonds between fibers under compression, which generate contractile forces upon network decompression. Compressive deformation appears to be a particularly effective way to reinforce networks compared to tensile and shear loading[13,49,50], perhaps due to increased contacts formed when fibers buckle under compression. Our computational model shows that the rigidity of fibrous networks can be tuned over a wide range as a consequence of the inherent sensitivity of the stiffness of fibrous networks to mechanical stress. This behavior provides a powerful way to program fibrous networks and tune their stiffness to diverse mechanical loading requirements. We expect this finding to be transferable to both tissue scaffolding proteins like collagen[19], and to cell scaffolding proteins like actin, which forms fiber bonds via cross-linking proteins[51]. In the latter case, remodeling emerges from redistribution of diffusible cross-linkers rather than from the formation of contacts between intrinsically cohesive fibers[15]. Since our minimal model shows that the only ingredient needed to achieve programmable mechanics is fibers that are stiff and cohesive, this bioinspired design principle can be readily carried over to synthetic self-reinforcing materials us-

ing any of a wide range of available synthetic fibers, including carbon nanotubes and cellulose nanofibrils[52,53].

6 Acknowledgments

This work is part of the research program of the Netherlands Organisation for Scientific Research (NWO). G.H.K. acknowledges support from the Foundation for Fundamental Research on Matter (FOM Program grant nr 143). F.C.M. was supported in part by the National Science Foundation (Grant PHY-1427654).

References

1 R. H. Pritchard, Y. Y. Shery Huang and E. M. Terentjev, Soft Matter, 2014, **10**, 1864.
2 R. C. Picu, Soft Matter, 2011, **7**, 6768.
3 J. Maxwell, Philosophical Magazine, 1864, **27**, year.
4 C. P. Broedersz, X. Mao, T. C. Lubensky and F. C. MacKintosh, Nature Physics, 2011, **7**, 983–988.
5 A. Sharma, A. J. Licup, K. A. Jansen, R. Rens, M. Sheinman, G. H. Koenderink and F. C. MacKintosh, Nature Physics, 2016, 3–7.
6 A. J. Licup, S. Münster, A. Sharma, M. Sheinman, L. M. Jawerth, B. Fabry, D. A. Weitz and F. C. MacKintosh, Proceedings of the National Academy of Sciences, 2015, **112**, 201504258.
7 A. J. Licup, A. Sharma and F. C. MacKintosh, Physical Review E, 2016, **93**, 012407.
8 M. L. Gardel, J. Shin, F. C. MacKintosh, L. Mahadevan, P. Matsudaira and D. A. Weitz, Science, 2004, **304**, 1301–1305.
9 C. Storm, J. J. Pastore, F. C. MacKintosh, T. C. Lubensky and P. A. Janmey, Nature, 2005, **435**, 191–194.
10 A. Dittmore, J. Silver, S. K. Sarkar, B. Marmer, G. I. Goldberg and K. C. Neuman, Proceedings of the National Academy of Sciences, 2016, **113**, 201523228.
11 A. D. Araújo, A. Majumdar, H. Parameswaran, E. Yi, J. L. Spencer, M. a. Nugent and B. Suki, Proceedings of the National Academy of Sciences of the United States of America, 2011, **108**, 9414–9419.
12 M. Gralka and K. Kroy, Biochimica et Biophysica Acta, 2015, **1853**, 3025–3037.
13 N. A. Kurniawan, B. E. Vos, A. Biebricher, G. J. Wuite, E. J. Peterman and G. H. Koenderink, Biophysical Journal, 2016, **111**, 1026–1034.
14 M. Knight, T. Toyoda, D. Lee and D. Bader, Journal of Biomechanics, 2006, **39**, 1547–1551.
15 K. M. Schmoller, P. Fernández, R. C. Arevalo, D. L. Blair and A. R. Bausch, Nature communications, 2010, **1**, 134.
16 H. López-Menéndez and J. F. Rodríguez, Journal of the Mechanics and Physics of Solids, 2016, **91**, 28–39.
17 P. Fernández and A. Ott, Physical Review Letters, 2008, **100**, 238102.
18 S. Münster, L. M. Jawerth, B. A. Leslie, J. I. Weitz, B. Fabry and D. A. Weitz, Proceedings of the National Academy of Sciences of the United States of America, 2013, **110**, 12197–202.
19 S. Nam, K. H. Hu, M. J. Butte and O. Chaudhuri, Proceedings of the National Academy of Sciences, 2016, **113**, 201523906.
20 L. Wolff, P. Fernandez and K. Kroy, New Journal of Physics, 2010, **12**, 053024.
21 M. W. Mosesson, Journal of Thrombosis and Haemostasis, 2005, **3**, 1894–1904.
22 A. S. G. van Oosten, M. Vahabi, A. J. Licup, A. Sharma, P. A. Galie, F. C. MacKintosh and P. A. Janmey, Scientific Reports, 2016, **6**, 294–299.
23 O. V. Kim, R. I. Litvinov, J. W. Weisel and M. S. Alber, Biomaterials, 2014, **35**, 6739–49.
24 H. C. G. de Cagny, B. E. Vos, M. Vahabi, N. A. Kurniawan, M. Doi, G. H. Koenderink, F. C. MacKintosh and D. Bonn, Physical Review Letters, 2016, **117**, 217802.
25 I. K. Piechocka, R. G. Bacabac, M. Potters, F. C. Mackintosh and G. H. Koenderink, Biophysical journal, 2010, **98**, 2281–9.
26 N. A. Kurniawan, J. Grimbergen, J. Koopman and G. H. Koenderink, Journal of Thrombosis and Haemostasis, 2014, **12**, 1687–1696.
27 P. Żeliszewska, A. Bratek-Skicki, Z. Adamczyk and M. Cieśla, Langmuir, 2014, **30**, 11165–11174.
28 C. P. Broedersz and F. C. MacKintosh, Soft Matter, 2011, **7**, 3186–3191.
29 S. B. Lindström, D. A. Vader, A. Kulachenko and D. A. Weitz, Physical Review E, 2010, **82**, 051905.
30 J. C. Maxwell, The London, Edinburgh, and Dublin Philosophical Magazine and Journal of Science, 1864, **27**, 294–299.
31 J. Wilhelm and E. Frey, Physical review letters, 2003, **91**, 108103.
32 M. Sheinman, C. P. Broedersz and F. C. MacKintosh, Physical Review Letters, 2012, **109**, 238101.
33 S. Alexander, Physics reports, 1998, **296**, 65–236.
34 M. Dennison, M. Sheinman, C. Storm and F. C. MacKintosh, Phys. Rev. Lett., 2013, **111**, 095503.
35 P. Rosakis, J. Notbohm and G. Ravichandran, Journal of the Mechanics and Physics of Solids, 2015, **85**, 16–32.
36 O. Chaudhuri, S. H. Parekh and D. A. Fletcher, Nature, 2007, **445**, 295–298.
37 L. D. Landau and E. M. Lifshitz, Theory of Elasticity, Pergamon Press, 1986.
38 K. John, D. Caillerie, P. Peyla, A. Raoult and C. Misbah, Physical Review E, 2013, **87**, 042721.
39 X. Xu and S. A. Safran, Physical Review E, 2017, **95**, 052415.
40 S. Alexander, Physics Reports, 1998, **296**, 65–236.
41 M. Sheinman, C. P. Broedersz and F. C. MacKintosh, Physical Review E, 2012, **85**, 1–16.
42 N. Laurens, R. P. C. Driessen, I. Heller, D. Vorselen, M. C. Noom, F. J. H. Hol, M. F. White, R. T. Dame and G. J. L. Wuite, Nature communications, 2012, **3**, 1328.
43 J. van Mameren, M. Modesti, R. Kanaar, C. Wyman, E. J. G. Peterman and G. J. L. Wuite, Nature, 2009, **457**, 745–748.
44 A. D. Protopopova, N. A. Barinov, E. G. Zavyalova, A. M. Kopylov, V. I. Sergienko and D. V. Klinov, Journal of Thrombosis and Haemostasis, 2015, **13**, 570–579.

45 R. I. Litvinov, S. Yakovlev, G. Tsurupa, O. V. Gorkun, L. Medved and J. W. Weisel, Biochemistry, 2007, **46**, 9133–9142.

46 C. P. Broedersz and F. C. Mackintosh, Reviews of Modern Physics, 2014, **86**, 995–1036.

47 P. R. Onck, T. Koeman, T. Van Dillen and E. Van Der Giessen, Physical Review Letters, 2005, **95**, 19–22.

48 E. Conti and F. MacKintosh, Physical Review Letters, 2009, **102**, 088102.

49 M. E. Susilo, J. A. Paten, E. A. Sander, T. D. Nguyen and J. W. Ruberti, Interface focus, 2016, **6**, 20150088.

50 U. Cheema, C. B. Chuo, P. Sarathchandra, S. N. Nazhat and R. A. Brown, Advanced Functional Materials, 2007, **17**, 2426–2431.

51 K. E. Kasza, A. C. Rowat, J. Liu, T. E. Angelini, C. P. Brangwynne, G. H. Koenderink and D. A. Weitz, Current Opinion in Cell Biology, 2007, **19**, 101–107.

52 V. A. Davis, A. N. G. Parra-Vasquez, M. J. Green, P. K. Rai, N. Behabtu, V. Prieto, R. D. Booker, J. Schmidt, E. Kesselman, W. Zhou, H. Fan, W. W. Adams, R. H. Hauge, J. E. Fischer, Y. Cohen, Y. Talmon, R. E. Smalley and M. Pasquali, Nature Nanotechnology, 2009, **4**, 830–834.

53 R. T. Olsson, M. a. S. Azizi Samir, G. Salazar-Alvarez, L. Belova, V. Ström, L. a. Berglund, O. Ikkala, J. Nogués and U. W. Gedde, Nature nanotechnology, 2010, **5**, 584–8.

We report that networks of the biopolymer fibrin can be reinforced by compression-decompression through strain-induced bonds, by building in stresses in the network.